Journal of Terramechanics 110 (2023) 87–99

Contents lists available at ScienceDirect

Journal of Terramechanics

journal homepage: www.elsevier.com/locate/jterra

Push-pull locomotion: Increasing travel velocity in loose regolith via induced wheel slip ☆

Cyndia Cao [a,*], Deaho Moon [a], Colin Creager [b], Dennis K. Lieu [a], Hannah S. Stuart [a]

[a] University of California, Berkeley, 2521 Hearst Ave, Berkeley, CA 94709, USA
[b] NASA Glenn Research Center, 21000 Brookpark Rd, Cleveland, 44135 OH, USA

ARTICLE INFO

Article history:
Received 8 May 2023
Accepted 22 August 2023

Keywords:
Planetary rover
Slip control
Granular resistive force theory
Push–pull locomotion
Sandy slopes

ABSTRACT

Push–pull locomotion is an effective mobility mode for traversing loose lunar regolith and climbing sandy slopes. A rover with an active suspension can generate thrust from a set of anchored wheels by adjusting its wheelbase while driving the remaining wheels. This paper explores the relationship between the velocities of the rotational and translational suspension elements. Using a kinematic slip greater than 30%–40%, inchworming surpasses both the travel velocity and power efficiency of normal driving on slopes between 10°–20°. On a 20°slope, inchworming improves travel reduction from 98% to 85% and reduces normalized power consumption by a factor of eight. Experiments with NASA's upcoming Volatiles Investigating Polar Exploration Rover show that increasing kinematic slip increases its travel velocity in a sink tank by 35%. Models using granular resistive force theory indicate that wheels driving at higher slip can generate greater tractive force and thus reduce the load on the anchored wheels. Otherwise, at lower driving slip, the load capacity of anchored wheels may be exceeded and result in oscillatory overall travel. These experiments suggest that there is further room to improve wheeled locomotion by intentionally inducing wheel slip, especially in articulated suspensions.

1. Introduction

Planetary rovers have a history of entrapment in soft sand on Mars, which is difficult to remotely or visually anticipate because terrain properties are influenced by hidden, sub-surface composition (Chhaniyara et al., 2012). On-board slip detection is still an open research field, which makes it challenging to respond to impending entrapment (Gonzalez and Iagnemma, 2017). Future missions are planned to other challenging low-gravity terrains. NASA will return to the moon to scout lunar craters for water ice and other resources via the Volatiles Investigating Polar Exploration Rover (VIPER) (NASA). Unfortunately, studies have shown that mass-scaled testing on Earth cannot fully capture the looseness of soil in reduced gravity (Niksirat et al., 2020). VIPER specifically will dip into and around potentially loose permanently-shadowed craters, and speed will be essential to ensure access to time-dependent solar power and communications (Shirley et al., 2022). As exploration of the moon increases, locomotion on loose, sandy or regolith-covered slopes will impact more missions and incentivizes the design of more energy-efficient locomotion suspensions and gaits.

1.1. Push–pull locomotion

Push–pull locomotion has been studied extensively, notably using the rovers Scarab (Creager et al., 2015) and ExoMars (Azkarate et al., 2015). These rovers can expand and contract their suspensions such that they alternately drive half of their wheels while creating a platform or anchor with the other half. Bouton and Gao (2022) built a rover with a series of joints controlled in the yaw and roll directions that separate the front and back halves of the chassis. This rover's "squirming" gait is not strictly a push–pull gait but can generate similar effects as it twists its suspension and synchronously varies its wheel velocities.

Scarab has four wheels; its front wheels are paired against its back wheels, creating a specific push–pull gait called inchworming, which is shown in Fig. 1. In the suspension expansion phase, the front wheels drive while the back wheels provide a stationary platform to push against. In the contraction phase, the back wheels drive while the front wheels provide a platform to pull towards. For a single wheel driving in high sinkage Fillite, Moreland

☆ This work was supported by a NASA Space Technology Research Fellowship [Grant #80NSSC19K1167].
* Corresponding author.
E-mail addresses: cyndia_cao@berkeley.edu (C. Cao), dmoon@berkeley.edu (D. Moon), colin.m.creager@nasa.gov (C. Creager), dlieu@berkeley.edu (D.K. Lieu), hstuart@berkeley.edu (H.S. Stuart).

https://doi.org/10.1016/j.jterra.2023.08.005
0022-4898/

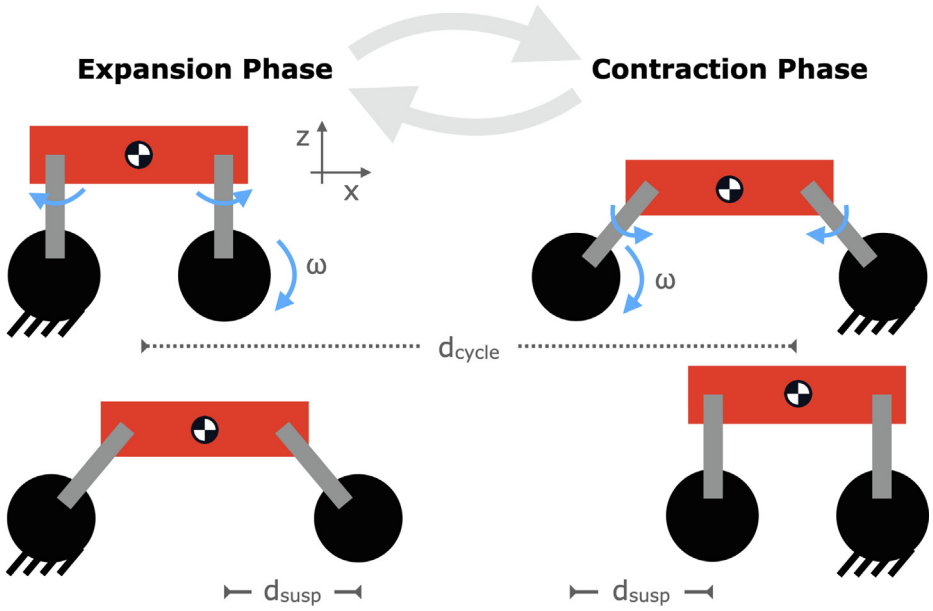

Fig. 1. Push–pull locomotion, or inch-worming, gait. During each phase, one set of wheels remains stationary to act as a platform while the remaining wheels drive at speed ω and the suspension expands linearly by distance d_{susp}. The rover overall moves by d_{cycle} each cycle.

(2013) measured a drawbar coefficient, or net thrust normalized by wheel load, of 0.32 when the wheel was locked and pushed on in comparison to -0.10 when driven at 20% slip. Shear Interface ImagingAnalysis showed that the displacement of grains behind a non-driving wheel is consistentlyhorizontal, whereas driving wheels excavate grains with their rotational motion (Skonieczny et al., 2014).

del Pulgar et al. (2019) evaluated the power efficiency of a push–pull gait compared to normal driving for the ExoMars rover and delineated ranges of terrain properties and slope angles for which it would be preferable to operate in each mode. As the media gets looser and the slope gets steeper, push–pull locomotion enables mobility, whereas on flat or benign terrains, push–pull locomotion draws excessive power. Other notable extrication gaits include the swimming gait of RP-15 (Shrivastava et al., 2020) and the squirming gait of MARCEL (Bouton and Gao, 2022). The squirming gait consists of oscillatory yaw control between the front and back halves of the rover; one wheel is held stationary as the others drive synchronously with the internal steering. Bouton et al. (2023) built two rovers with a consistent weight and wheel design to explicitly compare many modes of push–pull locomotion, including squirming, inchworming, wheel-walking, with passive and fixed suspensions. However, all wheel speeds in the experiment were driven at angular velocities that are synchronous with each suspension gait, producing theoretical no-slip translation.

Our present paper explores the critical role of purposefully induced wheel slip in generating thrust in high sinkage, loose granular media.

1.2. Terramechanics modeling

Several empirical and simulation-based methods exist for predicting mobility behavior in granular media, including the traditional Bekker-Wong model (Bekker, 1969), continuum methods (Agarwal et al., 2019), and Discrete Element Methods, in order of increasing computational complexity. The granular Resistive Force Theory (RFT) method is a simple empirical model that depends on a single measured terrain parameter to predict the forces experienced by an object moving through cohesionless sand (Li et al., 2013). RFT can predict the drawbar pull, sinkage, and wheel torque of a single fixed-slip wheel at an accuracy similar to or better than the Bekker-Wong model (Agarwal et al., 2019).

The extension of RFT to 3D objects and trajectories (Treers et al., 2021; Agarwal et al., 2023) allows the application of the model to a wider variety of motions, suspension kinematics, and wheel geometries than traditional empirical models. RFT was used to evaluate a locomotion gait of the RP-15 rover (Shrivastava et al., 2020), which was an early motivation for the kinematic design of VIPER. RFT also allows rover designers to consider the effect of gravity on locomotion, since the mechanical strength of granular media changes with gravity. Slonaker et al. (2017) developed non-dimensionalized scaling laws based on RFT that account for wheel diameter, mass, and gravity levels and verified these in DEM simulation. Daca and Skonieczny (2022) found that RFT's gravity dependence conservatively estimates mobility metrics within 30% error during single-wheel experiments in Martian and lunar gravity on reduced-gravity flights.

Push–pull locomotion specifically depends on using the non-driving wheels as platforms or anchors to generate thrust from. Frequently in practice, the forces on the anchored wheel can exceed the shear strength of soil, resulting in backwards anchor displacement and oscillatory overall motion. In the past, hand-tuning was done to find control inputs that work, but limit surfaces enable more methodical predictions and control. RFT-generated limit surfaces can predict the load bearing capacity of an object in sand (Huh et al., 2023). RFT therefore holds potential for predicting the efficacy of non-driving or anchored wheels.

Both RFT and the Bekker-Wong equations model the forces on a wheel as dependent on slip and sinkage and independent of velocity. This relationship as predicted by RFT is depicted for one of VIPER's round, rigid, 50 cm diameter wheels in 2(a). Both these models and experimental single-wheel drawbar pull tests show that the net tractive force at 0 slip is negative; positive slip is required to generate positive tractive force. Fig. 2(b) shows slices of the contour plot shown in Fig. 2(a) at different levels of wheel sinkage. For benign levels of sinkage, the drawbar pull plateaus once the wheel reaches a slip of about 20%. As sinkage increases, the slope of the drawbar pull curve is more positive, which allows

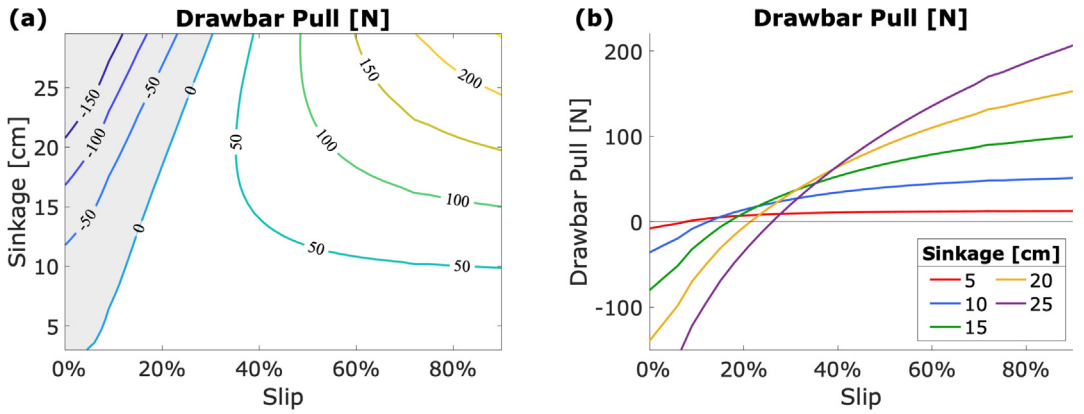

Fig. 2. (a) Drawbar pull as predicted by RFT for varying levels of wheel sinkage and slip for a VIPER wheel, adapted from Cao et al. (2021). The model is for a cohesionless sand with a generic RFT scaling coefficient, which can be proportionally scaled up for a dense media or scaled down for a loose media. In the gray region, resistance is greater than thrust, resulting in negative net tractive force. (b) Slices of the contour plot in (a) for various fixed levels of wheel sinkage (disregarding wheel load). As wheel sinkage increases, greater slip is required to maintain net positive traction. At low sinkage, the drawbar pull plateaus after 20–30% slip, whereas at very high sinkage, i.e. up to the axle (25 cm), drawbar pull continues to increase significantly with greater slip.

the wheel to continue generating additional traction by increasing slip.

Traditional slip controllers try to minimize or coordinate slippage between wheels, but experiments in Cao et al. (2021) showed that driving the front and back wheels at different speeds against high towing forces could improve traverse velocity due to the different sinkage of each pair of wheels. However, this observed effect was limited by the fixed suspension of the test rover used. The present paper shows that, for articulated suspensions capable of push–pull locomotion, strategically inducing slip in high sinkage media increases traction and substantially improves vehicle performance.

1.3. Overview

In this work, we evaluate the relationship between driving wheel slip and mobility performance on a variety of slopes. In Section 2, we perform comprehensive tests on a shoebox-sized rover climbing a sandy slope up to 20°using a range of wheel slips. In Section 3, we present data from four extrication trials by the VIPER lunar rover in an extreme high-sinkage simulant. In Section 4, we use RFT to estimate the forces on the wheels and predict whether or not the anchored wheels can sustain the load on them in order to resist skidding. Finally, in Section 5 we suggest how this research may influence suspension design and can be used to evaluate or improve the performance of real rovers.

2. Sloped driving experiments

Shifty, pictured in Fig. 3, is a four wheel rover weighing 9.7 kg with the kinematics shown in Fig. 1. It has a 27.2 cm minimum wheelbase, 13.1 cm suspension legs, and 17.5 cm wheels. Based on the scaling laws presented in Slonaker et al. (2017), the rover's performance is scalable to a 360 kg rover with 50 cm wheels on the moon, which would be similar to that of VIPER.

To quantify the relationship between rotational and translational inputs, we define a quantity called kinematic slip, which is equivalent to the wheel slip of the driving wheel assuming the anchored wheel stays fixed in place. Wheel slip is traditionally defined as:

$$s = 1 - \frac{v}{\omega r} \tag{1}$$

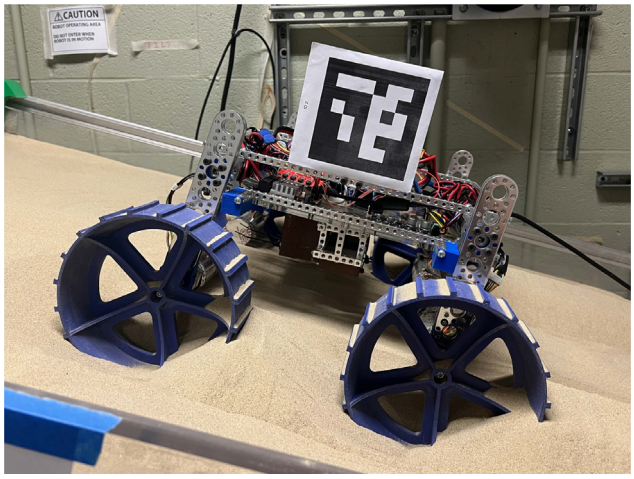

Fig. 3. Shifty driving in its minimum wheelbase configuration up a 15°slope.

where v is the wheel's achieved linear velocity, ω is the rotational velocity, r is the radius, and ωr is the theoretical maximum no-slip translational velocity of the wheel. Kinematic slip is hence defined as

$$ks = 1 - \frac{d_{susp}}{\omega r t_{cycle}/2} \tag{2}$$

where d_{susp} is the linear travel of the suspension as defined in Fig. 1 and $t_{cycle}/2$ is the time of one gait phase. This results in an average measure of slip over the gait, rather than an instantaneous slip, which changes depending on Shifty's leg angle. The kinematic slip is equal to the ground-relative slip of the driving wheel only when the anchored wheel does not skid.

Experiments with Shifty comprise inchworming gaits with varying kinematic slip on a range of slopes up to 20°. These are compared to normal driving to characterize the efficiency of inchworming while climbing sandy slopes. Several representative videos are included in the supplemental materials.

2.1. Experimental setup

The tiltable sandbox is filled with Mars 90, which Oravec et al. (2021) found to best match the known mechanical properties of

Martian wind-drift soil out of readily available lunar and Martian simulants. The looseness of wind-drift soil has posed significant slippage and entrapment challenges for Mars rovers, and Mars 90 is the baseline simulant used for mobility assessments of the Curiosity and Perseverance rovers.

We test a range of kinematic slips from 0% to 85% and slopes of 0°, 10°, 15°, and 20°. Five kinematic slips plus one normal driving condition are tested for each slope with a wheel velocity equivalent to the 60% kinematic slip drive velocity. The non-driving wheels are unpowered while the driving wheels are velocity-controlled to a constant speed. Three trials are performed for every test condition. The sand is stirred and then leveled between trials to reset any compaction that may have occurred, before being tilted to the test angle.

Fiducial markers attached to the tilt table and the rover are used to track the rover's motion. The motion of the wheels is calculated using a combination of the rover tracking data and onboard joint encoders. Current sensors on the input side of each motor controller measure the current consumed by each pair of legs and wheels separately.

Two datasets are taken, where the second dataset (dashed lines with triangle markers in Figs. 4,5) confirms the results of the first (solid lines with circle markers). In the second dataset, electrical current is measured over a larger range of amperage and true voltage measurements are used instead of a nominal estimate to support the initial results with higher fidelity. The wheel velocity controllers are also adjusted for the second trials to track the target velocity better. This results in a shift in the tested kinematic slip values, which are all calculated using the measured joint velocities.

2.2. Results & discussion

Tests of normal driving typically use wheel slip to evaluate mobility performance, where the velocities of all wheels are the same, resulting in the same value for wheel slip and overall vehicle travel reduction. Travel reduction *TR* for inchworming similarly quantifies the deviation of the vehicle's trajectory from its ideal trajectory by assuming that the anchored wheels are fully stationary and the chassis moves by the suspension expansion distance d_{susp} each cycle. Numerically,

$$TR = 1 - \frac{d_{cycle}}{d_{susp}} \tag{3}$$

where d_{cycle} is the actual travel distance of the rover's center of mass over one complete expansion–contraction cycle. These quantities are illustrated in Fig. 1. If the anchored wheel exceeds its load capacity and is pushed backwards, d_{cycle} will be less than d_{susp} and result in a positive travel reduction.

Fig. 4 shows both travel velocity and travel reduction as a function of the achieved kinematic slip. The tested slopes are distinguished by color and the two datasets are distinguished by markers and line dashes. The separate datasets show good agreement and the shaded region represents one standard deviation of error, both indicating that the results are replicable. The horizontal lines show the average travel reduction during normal driving trials, when all four wheels are driven at the same velocity without inchworming. The travel reduction of a normal driving trial is equivalent to slip as defined in Eq. 1.

Travel velocity increases as wheel slip increases but generally plateaus around 60% kinematic slip. Moreover, travel reduction on slopes is not improved beyond the baseline all-wheel-drive until 20–30% kinematic slip is introduced. Past this point, substantial gains can still be achieved, with 60–80% kinematic slip resulting in about half of the travel reduction of normal driving on 10°and 15°slopes. On the 20°slope, travel reduction is reduced from 98% to 85% using 70% kinematic slip.

Travel reduction captures the state of the rover, quantifying its efficiency and chance of entrapment, but the values plotted are defined differently for normal driving and inchworming and so are not an exact comparison. The most direct comparison is the power number *PN*, which is the power normalized by travel velocity and vehicle weight, or

$$PN = \frac{P}{vW}, \tag{4}$$

where *P* is the average power consumed, v is the average velocity travelled, and *W* is the weight of the vehicle. This quantity is unitless, which also allows us to compare it to other vehicles' performance.

As shown in Fig. 5, the power number is improved by high kinematic slip when driving on slopes, reaching better levels than normal driving once between 30–40% kinematic slip is applied. On 10°slopes, the power number is reduced by a factor of up to 3. On 20°slopes, the power number is reduced by a factor of up to 8.

These results also reconfirm previous findings that inchworming in benign terrains results in excessive and unnecessary energy consumption. Travel reduction while inchworming on flat sand (0°) is generally higher than the baseline driving slip of 0%. It only falls below 0% due to the mathematical definition of travel reduction, when the driving wheels generate so much tractive force that they drag the undriven wheels forwards, achieving higher velocity than solely from suspension actuation. Neither of these situations is efficient for locomotion and normal driving should be employed. The nature of the cyclical inchworming gait also means that the maximum achievable travel velocity is half the velocity achievable by driving all four wheels simultaneously on flat ground. Finally, inchworming on the flat ground draws at best 50% more energy than normal driving.

These relationships between kinematic slip and mobility are further explored via the VIPER rover's mass-scaled mobility test unit in the following section.

3. VIPER extrication experiments

NASA's Volatiles Investigating Polar Exploration Rover (VIPER) is designed to prospect the lunar south pole for water, ice, and other resources that can be harvested in future missions to support further space exploration (Smith et al., 2022). NASA aims for VIPER to drive 20 km on slopes of up to 15°in 100 Earth days, with a top speed of 0.2 m/s (0.45 mph). VIPER will drive around craters in permanently shadowed regions with highly uncertain terrain properties. These sites have not been previously visited and may include regolith that is looser than that found in the equatorial Apollo landing sites Metzger et al. (2018). Accordingly, rather than following the design history of NASA's Mars rovers with passive suspensions, VIPER's suspension incorporates additional degrees of actuation to prepare for a spectrum of mobility challenges.

3.1. Rover kinematics

VIPER has four wheels with three degrees of freedom at each of its wheel modules – suspension, steering, and drive – that allow VIPER to independently lift each wheel, turn in place, and drive in different directions without changing body orientation (also known as crabbing). VIPER's actuated suspension enables the rover to control both its body attitude and ground clearance to perform tasks such as lowering its science instruments to the surface. Load cells on the suspension also allow the rover to control the contact force at each wheel.

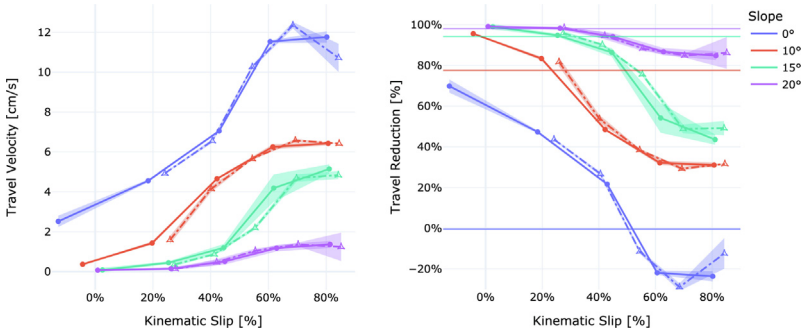

Fig. 4. Travel velocity and travel reduction. Travel velocity increases with increasing kinematic slip. Inchworming becomes more effective than normal driving (horizontal lines) on slopes after about 20–30% kinematic slip.

VIPER's suspension joints are actuated about its roll axis, which changes VIPER's track width when the wheels are steered in the rover's forward direction. This motion is perpendicular to the driving direction. Push–pull locomotion requires translation in the driving direction, so the wheels are steered as far as possible (45°) towards the suspension expansion direction to create a gait referred to as crab-worming. During each cycle, the suspension travels about 6 cm, but only 4.3 cm aligns with the wheel $+x$ direction. The resulting motion is depicted in Fig. 6. Kinematic slip as defined in Eq. 2 is modified to only consider wheel-aligned suspension motion.

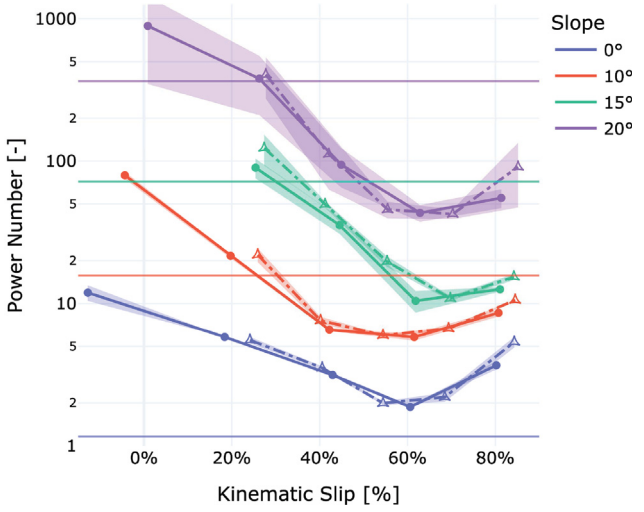

Fig. 5. Power number, or normalized energy consumption. Inchworming becomes more power efficient than normal driving on slopes after about 30–40% kinematic slip.

3.2. Experimental setup

The experimental rover is a mass-scaled mobility testbed of VIPER. In comparison to Shifty, which reaches 77% travel reduction on 10°slopes and 98% on 20°slopes in Mars 90, VIPER achieves approximately 15% travel reduction on 10°slopes and 75% on 20°-slopes in GRC-1 when performing normal driving.

To recreate extreme sinkage events at NASA Glenn Research Center (GRC), the Simulated Lunar Operations (SLOPE) Laboratory has a tank filled with Fillite (Tolsa Industrial), a material composed of hollow ceramic microspheres. The media is lightweight with low shear strength (Edwards et al., 2016) and quickly fills itself back in, so trials are run without preparing the media's surface. All four wheels are first driven at the same velocity until the chassis is embedded in the Fillite and no longer makes forward progress. Then the crab-worming gait is initiated in the opposite direction as the vehicle extricates itself, as shown in Fig. 7.

This process is repeated four times, with two trials of the baseline drive velocity of 0.3 rad/s and one trail each of drive velocities 0.5 rad/s and 0.7 rad/s. The suspension actuation speed is held constant across all cases. In the baseline case, the wheel drives slightly farther (7.5 cm) than the suspension expands each cycle (6 cm), but

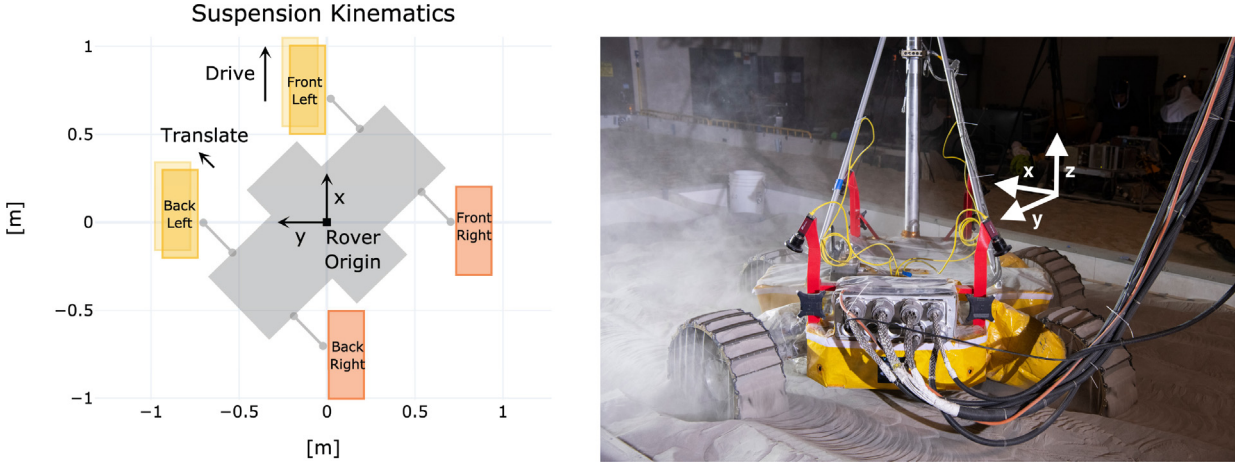

Fig. 6. VIPER kinematics. VIPER steers its wheels to 45°to maximize suspension travel alignment with the drive direction during its crab-worming gait. The left wheels (yellow) drive during the expansion gait while the right wheels (orange) drive during the contraction gait. The image on the right shows the Fillite sink tank at GRC.

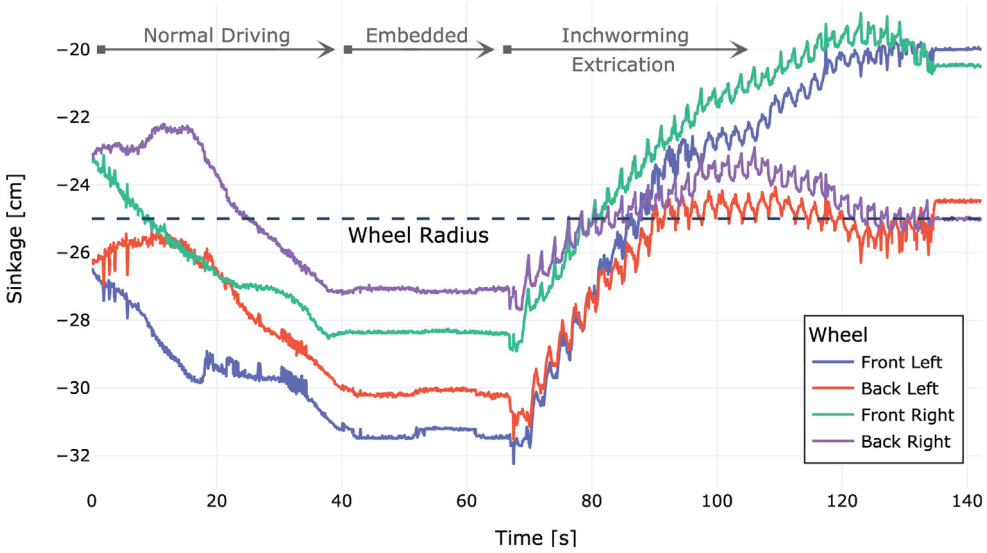

Fig. 7. Embedding and extrication during a single trial. All four of VIPER's wheels are driven until they sink past their axles and the chassis is fully embedded in the Fillite. Engaging the crab-worming gait enables the rover to extricate itself from entrapment and significantly reduce wheel sinkage during travel.

only about 70% of the suspension's travel is aligned with the wheel's x direction, resulting in about 35% kinematic slip.

SLOPE lab has 16 OptiTrack Prime^x 41 cameras mounted around the ceiling, and four Optitrack pucks on the chassis capture the motion of the rover (Schepelmann and Gerdts, 2022). Onboard encoders for each joint track their positions and velocities so that each individual wheel's motion can be estimated.

3.3. Mobility performance

Fig. 8 shows a top view of the progress achieved in the last 10 cycles of each test. The start of each expansion cycle is marked with a circle, while the start of each contraction cycle is marked with a triangle. The data are aligned with the forwards direction of the wheels ($+x$ in Fig. 6). The low slip cases result in the least travel, and the highest kinematic slip results in the fastest travel. Particularly visible in the red markers (36% kinematic slip), the rover's center of mass moves backwards during portions of the gait.

The outcome is summarized in Fig. 9. The high slip case (77% kinematic slip, 2.49 cm/s) results in 36% higher travel velocity than the baseline (35% kinematic slip, 1.83 cm/s). The drive velocity and kinematic slip are calculated from the actual joint values measured onboard, which is why the two 0.3 rad/s drive commands result in slightly different slips.

The energy required to move each meter decreases with higher kinematic slip but relative change is small (within 4% across all trials). While the high slip gait does not substantially improve energy efficiency as it did for Shifty, the results imply that efficiency is not sacrificed. Crab-worming (or any form of non-rolling locomotion) is a contingency gait for VIPER, which would only be triggered if the rover becomes entrapped. In such scenarios, there may be cases where travel velocity is critical to reach a location with access to solar power or communications. While instantaneous power draw would be higher for a high kinematic slip gait, the rover would not sacrifice overall energy consumption to reach its goal. The ability of crab-worming to extricate the vehicle reduces the risk of mission-ending entrapment, and the travel efficiency data give the mission operations team more mission planning flexibility and robustness should this situation be encountered.

Calculations of individual wheel travel per cycle in Fig. 10 show that the increase in net velocity results from both increased forwards travel of the driving wheels and decreased backwards skid of the anchored wheels. It is therefore interesting to understand when the anchored wheels are likely to skid because this hinders efficient travel. In the next section, we use RFT to explain and predict this effect.

4. Mobility models

Granular Resistive Force Theory can model the forces on a 3D wheel moving along a 3D trajectory[1]. We use RFT to estimate the forces on the wheels given their experimentally measured motions. Given a wheel's sinkage, we can also generate a load bearing capacity curve, or limit surface, and estimate where the rover is operating relative to this limit. In an efficient gait, the driving wheels should generate just enough traction not to skid the anchored wheels while also not dragging the anchored wheels behind them. We use the limit surface to characterize this range.

4.1. Estimated VIPER forces

Throughout this analysis, we estimate the RFT scaling coefficient of Fillite by picking a value to create agreement between the model's lift force and wheel torque outputs with the known weight of the vehicle and its drive torques as estimated from the motor current data.

Fig. 11 shows a sample of the calculated forces for one of VIPER's wheels in a (a) low slip (36%) case and (b) high slip (73%) case. Subfigure (i) shows the forces on the wheel during its driving phase, while (ii) shows the forces on the wheel during its anchored phase. The periodic black arrows with larger magnitudes show the forces on the grousers, which can provide substantially more thrust than the cylindrical wheel surface. The orange arrows show the velocity of the wheel, while the green arrows show the resultant force. In the low slip case (a)-(i), the sand in front of the wheel creates more resistance than traction, and the sand inside the wheel reduces lift. In the high slip case (b)-(i), the sand is more effectively displaced around the rim of the wheel and generates more net forward thrust. Subfigures (ii) in (a) and (b) show the

[1] Code for 3D RFT can be found here: https://github.com/embodied-dexterity-group/granular_rft_3D.

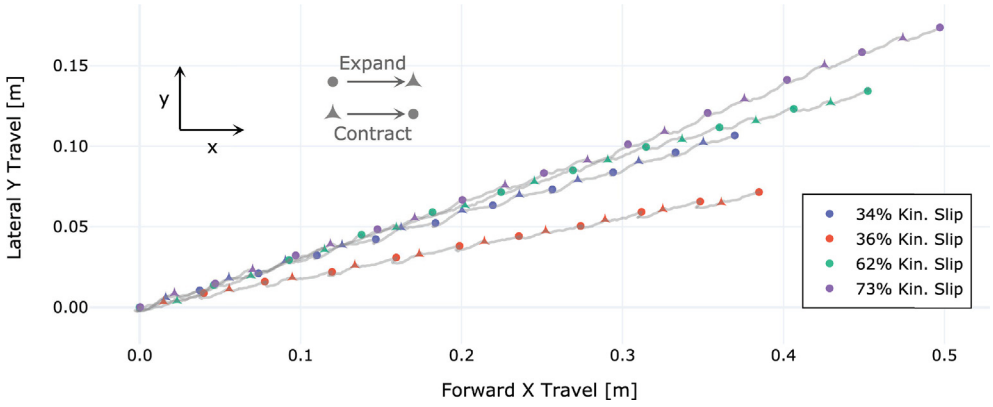

Fig. 8. Translation of the rover's origin over 10 crab-worming cycles. The beginning of each expansion cycle is marked with a circle, while the start of each contraction cycle is marked with a triangle. VIPER's wheels are oriented in the $+x$ direction.

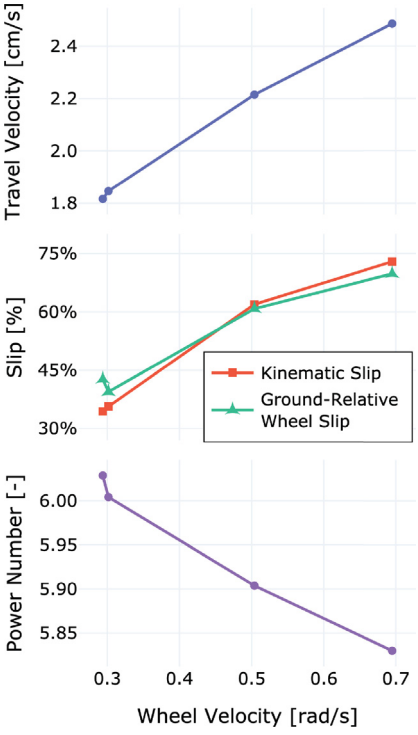

Fig. 9. Crab-worming mobility metrics. Kinematic slip correlates closely with ground-relative wheel slip, thereby providing a method to control slip rather than experience slip. By increasing kinematic slip, rover velocity is increased by 35% while slightly improving travel efficiency.

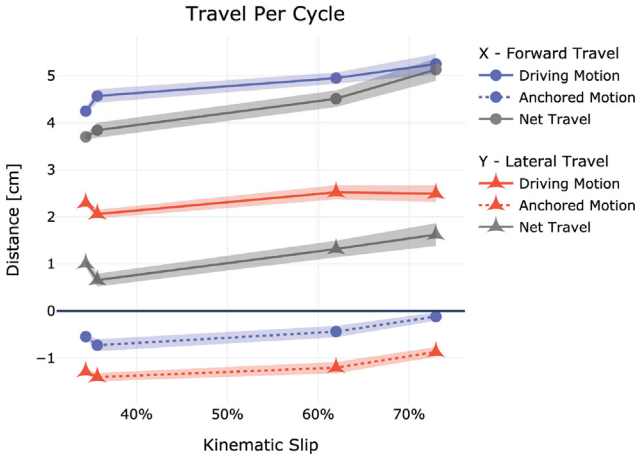

Fig. 10. Average longitudinal and lateral travel by each pair of wheels during each phase of the gait. The shaded error bars indicate one standard deviation of the travel over the last 10 cycles. Net travel is highest when the negative travel or anchor skid is minimized.

forces on the wheel during its anchored phase. In both cases, the anchored wheel is similarly effective at generating thrust and lift.

Subfigure (iii) shows the velocity of the wheel, which is determined by a combination of the Optitrack-measured chassis velocity and the encoder-measured kinematics of each wheel module. RFT uses these measured velocities to produce the estimated forces shown in (iv). The forces during the anchor phase are filtered by a moving average, since the low magnitude of the input velocity and its small variations cause large swings in output force due to the lack of velocity-dependence in the model. Each of the shaded errors bars in (iii) and (iv) are produced by the standard deviation over 10 cycles. The velocities and forces are consistent once the rover reaches steady state. Notably, the forward F_x force generated by the low slip wheel (a) during the driving phase is lower than the F_x in its anchor phase and much lower than the high slip driving F_x in (b).

Fig. 12 shows the resultant force profiles over all of the wheels, both over time each cycle (lines and shaded region) and on average over all time (markers with error bars). The left side subfigures, (a) and (c), show force generated by the driving wheels only, whereas the right side subfigures, (b) and (d), show the force generated by all wheels. The anchor forces by the stationary wheels will be overestimated by RFT because of the ruts left behind the wheels. However, this effect should be similar for all trials. The takeaways are that: (1) the tractive force generated by the faster-driving, higher-slip wheels is higher than that of lower-slip wheels; (2) the predicted average total forces are consistent across all slip conditions, which is expected given that the rover experiences the same external forces; and (3) the lateral resistance force F_y, which is a consequence of misalignment between the suspension and drive axes, decreases in magnitude with higher slip, resulting in less oscillation in y and more net translation.

The effect of (1) is that the anchor wheels skid backward less far in the x direction, and the effect of (3) is that there is less lateral force and travel oscillation in the y direction. Altogether, this results in faster travel when operating with high kinematic slip. The following load capacity analysis will substantiate these claims.

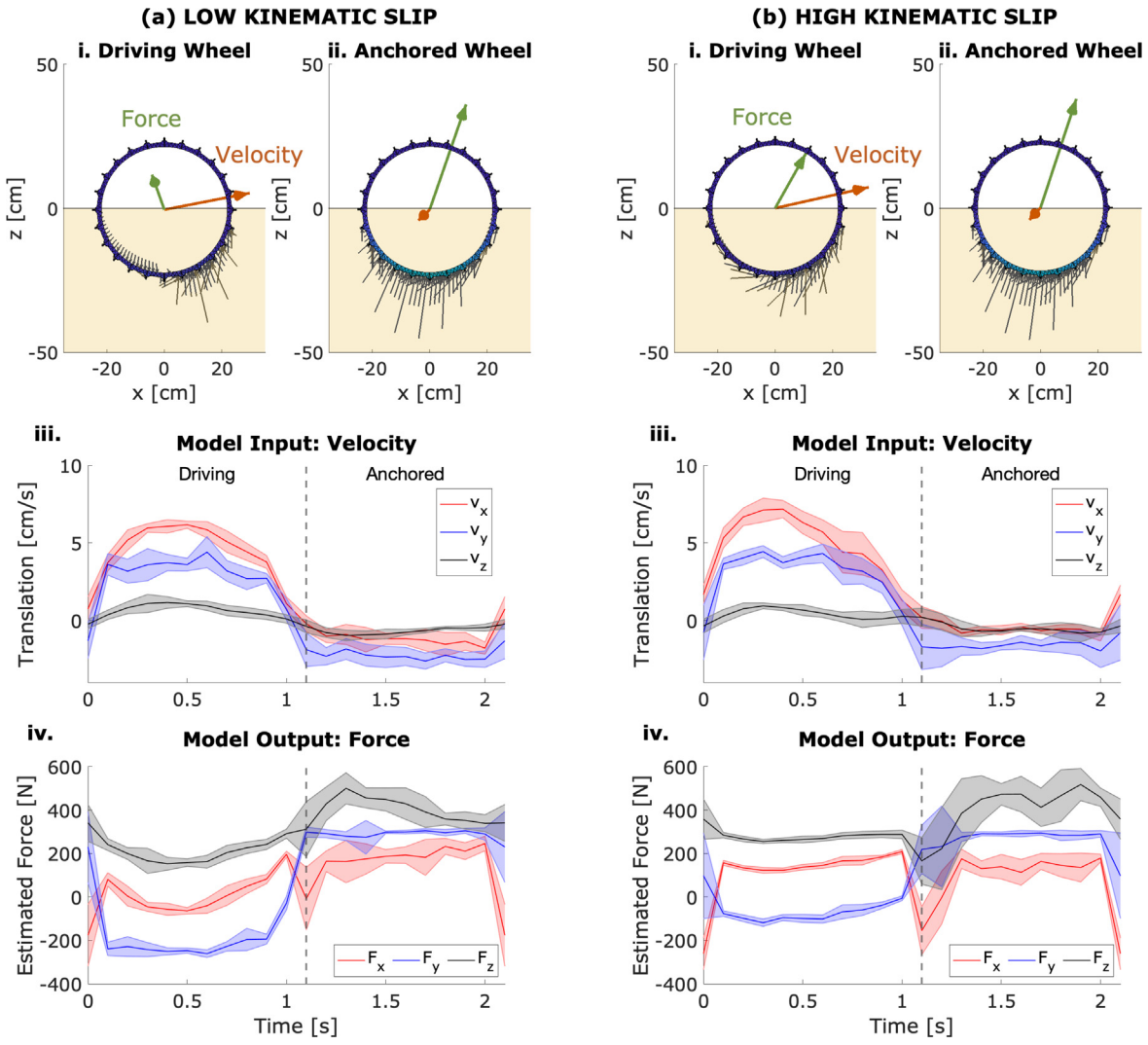

Fig. 11. The forces generated by one of VIPER's wheels when driven with the (a) lowest kinematic slip and (b) highest kinematic slip inputs, as predicted by RFT. The forward F_x force generated by the low slip wheel (a) during the driving phase is lower than both the F_x in its anchor phase and the F_x generated by driving with high slip (b).

4.2. Anchor load capacity for VIPER

RFT generates a velocity-independent estimate of the forces that resist a moving object. In reality, when the object begins to displace sand, the resistive load gradually increases until the sand compacts by some critical distance and subsequently produces a constant resistive force. Applying RFT to a sample of possible motion states of the object will generate a surface of potential resultant forces which represents the load capacity of the anchored object in granular media (Huh et al., 2023). Using this limit surface, we can predict the maximum force that the anchored wheels can support before the sand shears, and we can slip the driving wheels at a level that allows the anchored wheels to remain in place.

In the following analysis, we make several assumptions to reduce the complexity of the limit surface. First, there is no roll, pitch, or yaw motion of the rover – while there are a few degrees of yaw oscillation each cycle, the effect is small. Second, all four wheels are at a fixed and equal depth; the velocity of each wheel in the z direction is much lower than in the x and y directions. While there is some sinkage variation, the wheels are paired in the left and right direction, so the average sinkage of driving and anchored wheels is balanced, and the maximum observed difference is less than 5 cm in experiments (shown in Fig. 7). Finally, the terrain surface is assumed to be flat, whereas in reality there are variations as a cavity forms around the wheel during driving; this decreases the load capacity of a wheel being pushed backward.

In order to generate the limit surface shown in Fig. 13, horizontal translations (e.g. the red, green, and blue arrows) at different depths (red, green, and blue planes show the sand's surface) are applied to a mesh representation of the wheel. For each of these motions, RFT produces a point on the limit surface shown in (b)-(d). The red, green, and blue points show the forces generated by the red, green, and blue translations. A purely forward $+x$ translation (red) produces a purely backward $-x$ force, and a purely lateral $+y$ translation (blue) produces a purely lateral $-y$ force. The force increases as wheel submersion depth increases (green). Each circumferential contour line represents a depth increase of 2 cm, and each radial contour line represents a change in displacement direction by 15°.

To evaluate whether the rover is operating within the strength of the sand and the limit surface of the anchored wheels, we approximate the forces acting on the anchored wheel. Since the rover operates at low velocities, we approximate it as a quasi-static system such that the total net force is 0.

$$\sum F = F_{driving} + F_{anchor} - F_{resistance} = 0 \tag{5}$$

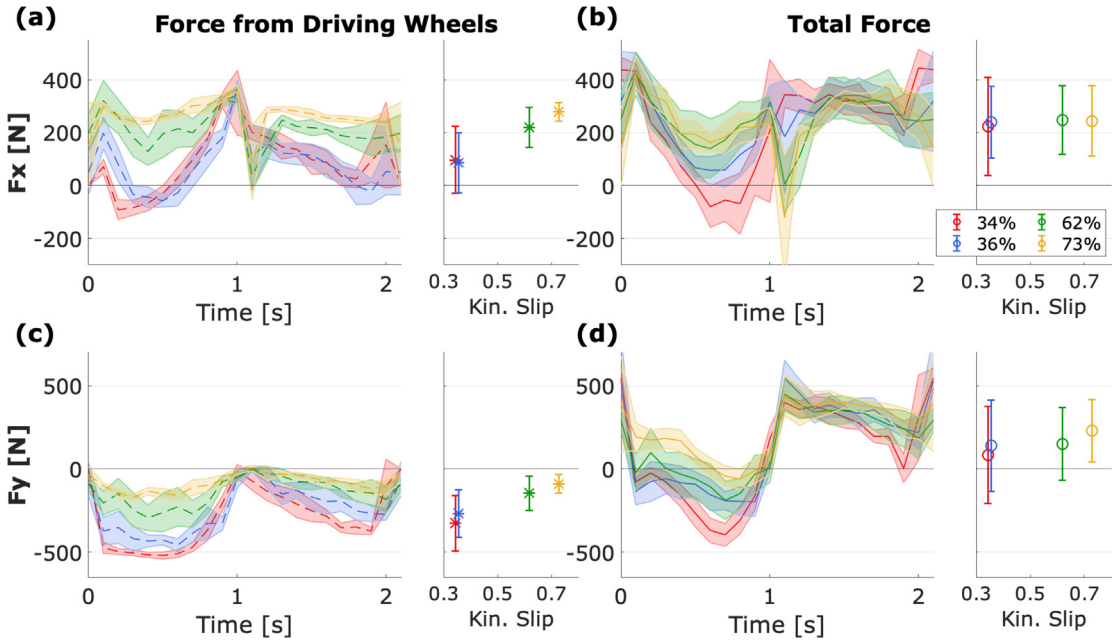

Fig. 12. Average forces in the forward (a)-(b) and lateral (c)-(d) directions. Subfigures (a) and (c) show the forces generated by only the driving wheels, while (b) and (d) show the total forces generated by all wheels. The shaded region depicts one standard deviation of the force time series over 10 cycles. The error bars show the range of forces (also one standard deviation) that is generated by the wheels over each entire cycle. As kinematic slip increases, the tractive force F_x of the driving wheels increases and the lateral resistive force F_y decreases.

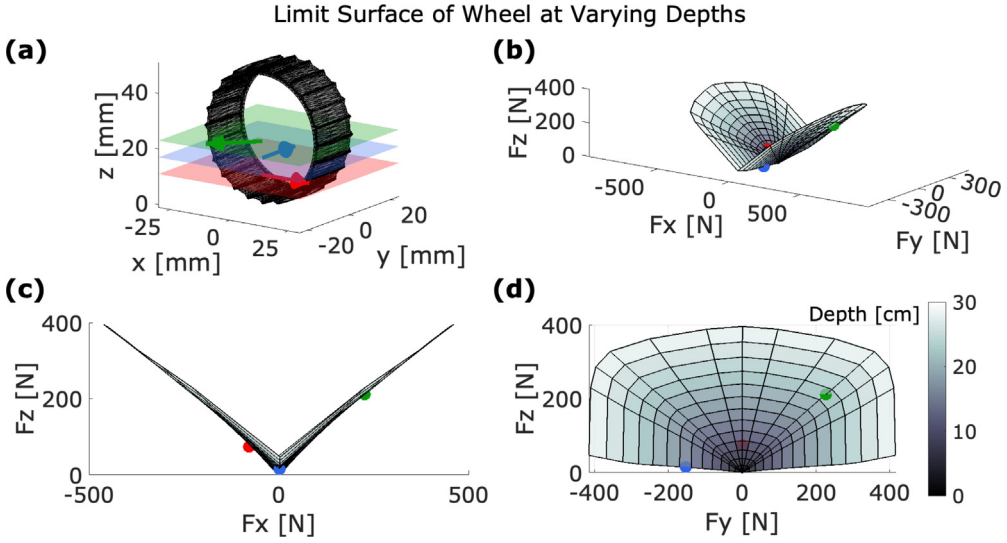

Fig. 13. Limit surface generation for the VIPER wheel shown in (a). The horizontal translations at varying depths denoted by the arrows and planes result in the forces on the limit surface (b)-(d) denoted by the points of the same color. Each circumferential contour line represents a depth increase of 2 cm, and each radial contour line represents a change in displacement direction by 15°.

where $F_{resistance}$ represents all external resistance forces that the model does not account for. This may include the energy dissipated into the Fillite that causes it to become airborne. Dynamic RFT suggests that wheel behavior should remain quasi-static under a velocity of 2 rad/s (Agarwal et al., 2021), but since the driving wheel operates at a maximum velocity of 0.7 rad/s, this modification would not affect the output of the model. The force difference may also result from over-estimation by RFT, since the wheels create surface variations and cavities in the Fillite that reduce the wheels' effective sinkage, which would reduce both the tractive performance of the driving wheels and the load capacity of the anchored wheels. Rearranged to isolate the anchored wheel, we see that the anchored wheels need to exactly counteract the resistance and driving wheel forces: $F_{anchor} = F_{resistance} - F_{driving}$. The average total force from Fig. 12 is the vehicle's $F_{resistance}$. Since the system is kinematically left–right symmetric, for the following analysis we only consider one pair of wheels, which includes one driving wheel and one anchored wheel.

Fig. 14 depicts the force that the anchor experiences F_{anchor} when different levels of kinematic slip are employed, each represented by a colored bubble. The center of the operating range is located at $F_{resistance} - F_{driving}$, where $F_{driving}$ is calculated assuming the anchor is fully stationary and the kinematics fully determine the wheel's translational motion. The shape of the bubble is gener-

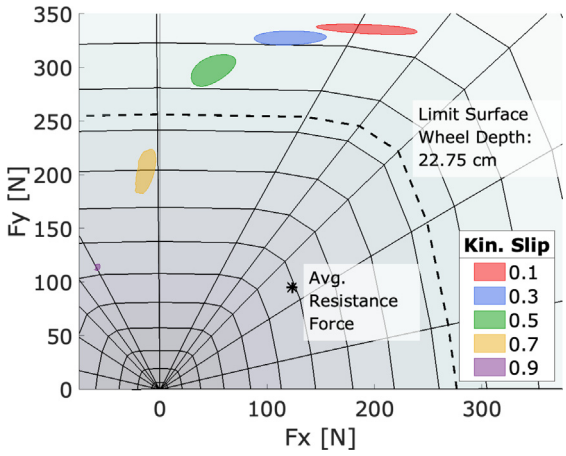

Fig. 14. The load acting on the anchored wheels given a driving kinematic slip (colorful bubbles) in comparison to the load capacity of those wheels (dashed line). A kinematic slip of at least 60% is required to operate within the limit surface of the anchored wheel. Each colorful bubble represents the range of F_{anchor} that is applied to the anchored wheel given the average external resistance force ($*$) and the force generated by the driving wheel, which depends on both the controlled kinematic slip and uncontrolled anchor skid. The size of the bubbles indicates the sensitivity of the driving wheel force generated to anchor displacement.

ated by accounting for potential anchor displacement and calculating the resultant variation of $F_{driving}$. We apply a fixed skid to the anchor in all directions with a velocity magnitude that is 10% of the suspension velocity. The shape of the bubble illustrates the sensitivity of the system to sliding of the anchor. For instance, for low kinematic slip, anchor skid results in substantial changes in forwards force F_x, whereas a high kinematic slip system is relatively insensitive and thus decreases operating uncertainty.

The dashed line shows the limit surface for the wheels at their average operating depth. A force on the anchor that is inside the dashed line should not cause anchor displacement, whereas a force outside the dashed line will have anchor skid. We only consider the x and y forces because the driving wheel generates similar lift forces as the anchored wheel and very little motion observed in the z direction. Kinematic slips of 10%, 30% and 50% impose forces on the anchor that fall outside the limit surface and will result in inefficient push–pull locomotion, since the anchor cannot support the load necessary to remain a stationary platform. Kinematic slips of 70% and 90%, however, allow the anchor to operate inside the limit surface so the anchored wheels would displace minimally. Note that all of the bubbles are fixed relative to $F_{resistance}$, marked by the $*$, so a different average resistance force would alter the location of the operating bubbles relative to the limit surface.

4.3. Comparing VIPER Model with experiments

The anchor behavior expected by Fig. 14 aligns with the experimental observations in Fig. 10, where approximately 70% kinematic slip is required to avoid anchor displacement. Kinematic slips at and below 62% result in less efficient push–pull locomotion due to the backward motion of the anchor, and a kinematic slip of 60% falls on the limit surface. While the model and experimental data generally agree on the boundary between anchor stability and anchor skid, the model over-estimates the stability of the anchor. This is likely due to several effects: (1) the average resistance force is a time-averaged estimate so it does not necessarily represent the worst-case moment in the cycle, and the instantaneous wheel slip also varies from the average slip that is modelled; (2) some sand must always be displaced in order to achieve its full strength under the anchor; (3) loads are unevenly distributed between the wheels, which are also at different sinkage, so one wheel may be within the limit surface while the other is not; and (4) the limit surface optimistically assumes flat terrain, whereas the cavity around the wheel reduces its load capacity until the wheel skids far enough to build up a mound.

Operating at 73% kinematic slip is within the limit surface and results in very little backward displacement, but it may not be the most efficient use of the anchored wheels. As mentioned above, sand often needs to displace by a critical distance before it achieves its full strength. If no anchor displacement occurs, the driving wheels are generating all of the vehicle's thrust. Additionally, in the 73% slip trial, one wheel was often dragged forward when it was not driving, which meant it created drag rather than providing thrust. This is not considered in the limit surface analysis, which ignores vehicle yaw. The power and travel velocity data still confirm that 73% slip resulted in the best mobility, but it is unlikely that performance would continue to improve with even higher slip.

Despite the assumptions and limitations of this model, the limit surface analysis is consistent with the trends observed during experiments. The ideal kinematic slip for VIPER in Fillite appears to be between 65–70% in order to operate within the limit surface while still taking advantage of the potential of the anchor to provide thrust.

In other media with different terrain properties, the shape of Fig. 14 would not change because the RFT coefficient equivalently scales the forces generated by the driving and anchor wheels. However, $F_{resistance}$ may shift and cause the ideal kinematic slip to change. In more consolidated media, wheel sinkage would decrease, shrinking the limit surface. Similarly, $F_{resistance}$ would decrease and bubbles of lower kinematic slip may into the limit surface. These new media would require more experimentation to characterize.

Note that the F_{anchor} operating ranges cross the limit surface primarily by exceeding F_y limits. This constrains the rover's potential to generate force in the x direction. If VIPER finds loose and sloped terrain and future missions expect to traverse it, then redesigning the suspension such that the expansion and contraction direction can align with the wheel drive direction would significantly reduce the amount of kinematic slip necessary to maintain a stationary anchor during push–pull locomotion, as suggested in Fig. 15. We next apply this analysis to the Shifty sloped climbing data.

4.4. Shifty & slope climbing

Combining both experimental datasets collected with Shifty, we can observe how anchor skid varies with kinematic slip in Fig. 16. For slopes of 0°and 10°, wheel travel by the front and back wheels is similar, and anchor travel is minimized near 40% slip. Beyond 40% kinematic slip, the non-driving wheels are dragged by the driving wheels, which is an inefficient use of tractive force. Mars 90 was not loose enough to warrant an inchworming gait when the terrain is flat. On the 10°slope, 40% slip is the level at which the inchworming power efficiency improves beyond normal driving and energy consumption plateaus around its minimum at less than half that of normal driving. On steeper terrain (15°and 20°), higher kinematic slip is required to reduce anchor motion. The rover achieves minimal back anchor skid around 60% kinematic slip, but the system is limited by front anchor skid. In this case, the front wheel cannot generate a strong enough platform to support the back wheels.

To produce Fig. 17, we perform a similar analysis as the previous section, comparing the operating force range with the limit surface. In each subfigure, the limit surface contours are the same, generated with a mesh model of Shifty's wheel, while the shifting

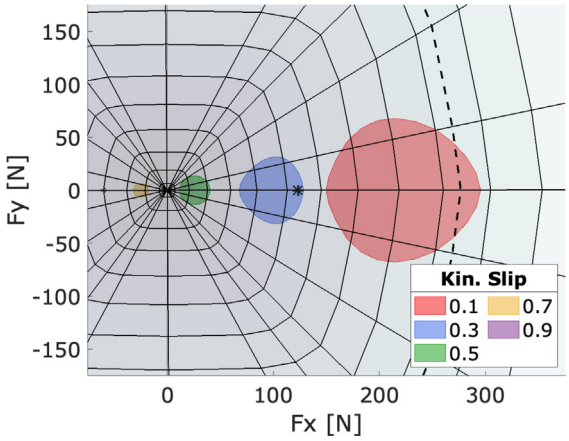

Fig. 15. The load acting on the anchored wheels given a driving kinematic slip in comparison to the load capacity of those wheels if the suspension travel was aligned with the driving direction. Much lower levels of kinematic slip would be required to remain within the limit surface.

dashed line indicates the limit surface for the average sinkage depth of the wheels on each slope. The forces are not scaled by a measured RFT coefficient because any changes in the shear strength of the sand due to its slope should be consistent and equally affect both wheels across every trial. The x axis is fixed to the rover's longitudinal or driving direction, rotating with the slope of the tilt table. We do not analytically account for how the gravity vector direction changes relative to the rover x and y axes; instead we use the average RFT-estimated total force to generate the $F_{resistance}$ $(*)$ values. As the slope increases, the average resistance force $F_{resistance}$ moves to the right in accordance with gravity, and this pushes the F_{anchor} bubbles closer to the limit surface. Therefore, the model captures why higher kinematic slip is necessary on higher slopes.

However, these model predictions do not correlate as clearly to Shifty's observed behavior, since the model predicts that most kinematic slip values are within the limit surface whereas anchor skidding occurs at many levels of kinematic slip. Many of the assumptions of RFT are not maintained as well in this experiment as with the flat tank of Fillite. RFT was characterized for a flat sandy surface, so it does not capture how slopes and surface topology variation affects locomotion. VIPER performed its crab-worming gait in a flat tank of Fillite, which easily reflows around the wheels compared to Mars 90. Meanwhile, Shifty's motion capture and kinematics data suggest that the front wheels sink more than the back wheels, but visual examination of the sand surface clearly confirms that the front wheels excavate the sand as they drive, which results in less effective sinkage, and then build a mound that increases the effective sinkage of the back wheels. In order for the model to capture reality more closely, front and back wheel sinkage would have to be adjusted to account for topology change, and a load capacity reduction factor or lower effective sinkage may be needed to represent the cavity created by a driving wheel.

Rather than attempting to increase model complexity, we instead use the shape of the limit surface to discuss the observed trends and use wheel displacement data to estimate where the anchored wheels operate in reality. Conceptually, we know that the limit surface increases in magnitude for wheels with greater sinkage. For the flat 0°terrain, the anchored wheel can be either dragged forward (positive travel) or pushed backward (negative travel) because the wheel sinkage is low and the load capacity is easily overcome. During sloped driving, wheel sinkage increases and since the anchored wheel has a larger limit surface, if it moves it always gets pushed backward, crossing only one side of the limit surface. Total resistance force increases on higher slopes due to the additional load imposed by gravity. This moves the anchor operating range bubbles rightward toward and across the dashed limit surface boundary. Hence, as observed, inchworming with low slip often exceeds the load capacity of the anchored wheel, whereas increasing kinematic slip reduces anchor displacement.

Based on the wheel travel data, the high kinematic slip bubbles for the 0°case should actually cross the limit surface in both the $+x$ and $-x$ direction, since the anchored wheels are pushed both ways. On the 10°slope, the anchored wheels do not appear to operate within the limit surface until about 50% kinematic slip. On the 15°and 20°slopes, the limit surface of the front wheel is always exceeded, whereas the back wheel remains in place at high kinematic slip. The substantial difference in front and back wheel

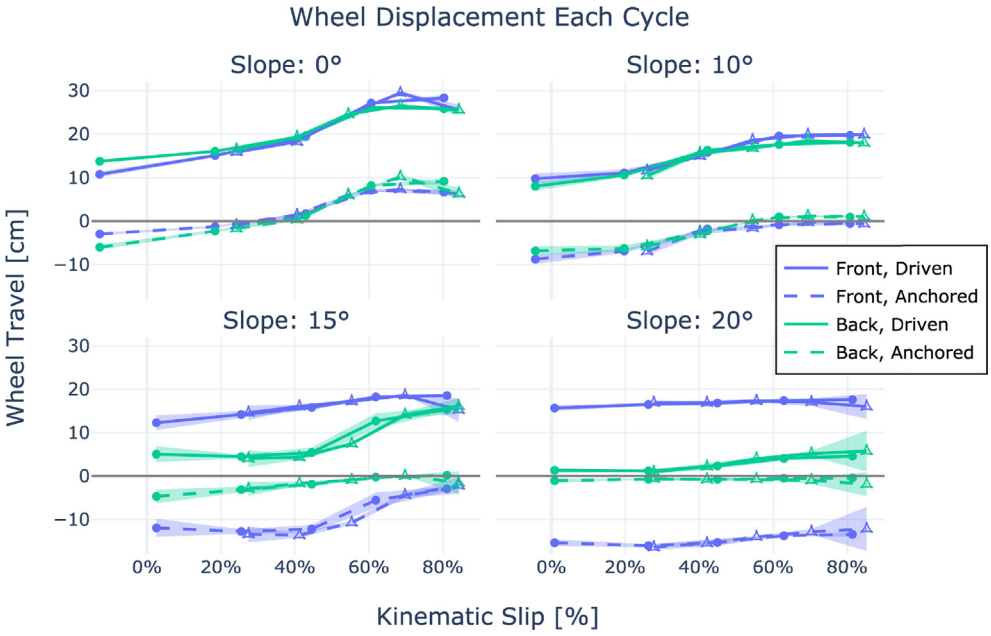

Fig. 16. Wheel displacement of Shifty during each phase of inchworming. At high slopes, the system is limited by front anchor skid; the front wheel cannot generate a strong enough platform to pull on the back wheels from.

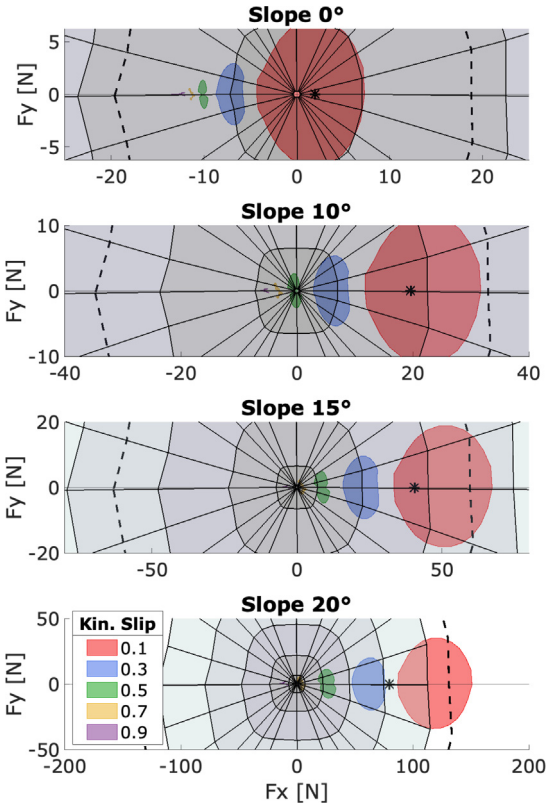

Fig. 17. Limit surfaces of Shifty's anchored wheels on varying slopes. Higher kinematic slip is necessary on higher slopes, but the actual magnitudes of the operating loads and the dashed limit surface cannot be captured by RFT because of the surface variations in the sand that are not accounted for. These figures are primarily useful for qualitatively considering how loads and load capacity are expected to change as the operating environment changes.

anchor capacity indicates that in order to enable more efficient slope climbing, future work should consider operating with different kinematic slip during the expansion and contraction phases, rather than keeping it constant throughout a given trial as in the present work.

5. Conclusion

In this work, experiments and theory demonstrated the great potential for improving the performance of push–pull locomotion gaits using purposeful wheel slip. Specifically, we investigated the crab-worming gait of VIPER and the inchworming gait of Shifty as case studies for this principle. Relative to normal driving, with inchworming we achieved an improvement in travel reduction from 98% to 85% on a 20°slope, from 94% to 44% travel reduction on a 15°slope, and from 77% to 30% travel reduction on a 10°slope. We found that the kinematic slip threshold to achieve less travel reduction than normal driving was between 20%-30% depending on the slope. The kinematic slip that resulted in more power efficient locomotion was between 30%-40%, reaching an efficiency improvement of between a factor of 3 for a 10°slope and a factor of 8 for a 20°slope. We achieved similar results on the VIPER rover in an extremely loose sand simulant. We first extricated the rover from an embedding incident and then, without increasing the normalized power consumption, increased travel velocity by 35% by increasing kinematic slip from 35% to 73%.

We also demonstrated the use RFT limit surfaces to visualize the theory behind the experimental results. We found that the higher slip driving wheels are more effective at generating positive tractive force and thus reduce the load on the anchored, non-driving wheels. This reduced the skid of the anchors, which resulted in more consistently forward locomotion. We also noticed that the suspension's kinematics and lateral motion generate a high F_y that limits the F_x that is achievable without overcoming the shear strength of the media. Unsurprisingly, an inchworming rover with its drive and suspension translation axes aligned would be a more effective kinematic design for continued access to loose, sandy slopes, compared with crab-worming. While we were limited by the assumptions of RFT from correlating theory to experiments for Shifty, we can still apply limit surface concepts to understand how kinematic slip should be adjusted to improve locomotion, given observations about the anchor skid states of the rover over a range of kinematic slips. This tool is therefore recommended as one method for considering the implications of new suspension kinematics and controllers in future rover applications.

6. Future work

Additional work is needed to further optimize push–pull locomotion gaits. Areas for development include improving simulation, implementing onboard sensing to inform responsive gait choices, and expanding experiments with induced slip in order to guide design and operation across diverse terrains.

The present RFT-based modeling method does not estimate the true mobility of Shifty, particularly due to the sloped terrain and surface variations in Mars 90. First, RFT is a rapid, first order model of forces on a moving body, whereas other more complex and time intensive simulation tools can more holistically predict performance, often with more granularity in the terrain specification. Some also consider multi-pass effects and sloped terrain, and they may be able to account for the surface topology effects that were encountered. Second, RFT depends on receiving motion tracking data as input to estimate the force. To answer the inverse problem and be able to predict the motion of a rover, either quasi-static (Huh et al., 2023) or dynamic simulations can be employed. These methods may be additionally able to account for vehicle weight distribution, which is affected by vehicle pitch on slopes and subsequently affects wheel loading and sinkage. RFT provided rapid visualizations useful for conceptual understanding of the role of slip, but more detailed simulation may be useful to reduce the experimentation required to characterize mobility over a large range of media.

In order to responsively initiate and optimize push–pull locomotion gaits with an effective level of slip as terrain changes, additional sensing should be explored. For example, a high level of travel reduction during normal driving could trigger a rover to transition from normal driving to push–pull locomotion, but slip estimation is still open area of research (Gonzalez and Iagnemma, 2017). Once inchworming is enabled, additional sensing would be useful to determine the proper level of kinematic slip. For an external observer, it is clear when the anchor skids and from the data, it is straightforward to pick a slip that minimizes skid. However, is is nontrivial to monitor the displacement of each anchor to allow for onboard adjustment of kinematic slip. Wheel sinkage may be easier to measure than skid and also provide insight into terrain properties to inform the desired wheel slip. However, more experiments to characterize the relationship between sinkage and load capacity are necessary to determine the feasibility of using sinkage measurements to make gait decisions. Alternatively, tractive force sensing at the wheel pairs may allow the operator to adjust kinematic slip until the measured load falls within an acceptable load capacity. It is expected that while the anchor is skidding, a relatively constant thrust force would be measured. Therefore, if kinematic slip is increased until a decrease in the thrust force is measured, this may be one sign that

the wheel has come within the media's load capacity. Increasing kinematic slip past this point would likely then result in less efficient thrust generation, especially if the measured force flips sign and becomes a form of resistance (i.e. dragging the anchor instead of pushing off the anchor). Furthermore, sensing of individual wheels would enable individual adjustment of kinematic slip, for instance between the expansion and retraction cycles or if there is local variation in terrain properties.

Even without additional simulation methods or sensors to measure robot state, future work should expand the experimental data set achieved in this work to include, for example, different kinematic slip between the expansion and contraction phases or more types of terrains. The effect of purposefully induced slip could also be explored with a wider variety of gaits, such as the squirming gaits in Bouton et al. (2023). Ultimately, the use of articulated suspensions provide operational flexibility for overcoming difficult terrains. At the same time, the deceptively simple choice of how fast to drive the wheels relative to that suspension can dramatically influence the effectiveness of such strategies. We found that induced wheel slip can be a locomotion tool, rather than an undesirable outcome. This introduces important design and control considerations for future rover configurations, which may include strategically inducing wheel slip, especially kinematic slip in articulated suspensions, for efficient locomotion in extreme and loose granular media.

Declaration of Competing Interest

The authors declare that they have no known competing financial interests or personal relationships that could have appeared to influence the work reported in this paper.

Acknowledgements

This work was supported by a NASA Space Technology Research Fellowship [Grant #80NSSC19K1167]. The authors would like to thank Arno Rogg and the rest of the VIPER mobility validation team for executing the extrication gaits presented in this paper.

Appendix A. Supplementary material

Supplementary data associated with this article can be found, in the online version, at https://doi.org/10.1016/j.jterra.2023.08.005.

References

Agarwal, S., Goldman, D.I., Kamrin, K., 2023. Mechanistic framework for reduced-order models in soft materials: Application to three-dimensional granular intrusion. Proc. Nat. Acad. Sci.120, e2214017120. URL: https://www.pnas.org/doi/abs/10.1073/pnas.2214017120, https://doi.org/10.1073/pnas.2214017120. publisher: Proceedings of the National Academy of Sciences.

Agarwal, S., Senatore, C., Zhang, T., Kingsbury, M., Iagnemma, K., Goldman, D.I., Kamrin, K., 2019. Modeling of the interaction of rigid wheels with dry granular media. J. Terrramech. 85, 1–14. https://doi.org/10.1016/j.jterra.2019.06.001.

Azkarate, M., Zwick, M., Hidalgo-Carrio, J., Nelen, R., Wiese, T., Joudrier, L., Visentin, G., 2015. First experimental investigations on wheel-walking for improving triple-bogie rover locomotion performances. In: ASTRA 2015, European Space Agency, Noordwijk, The Netherlands.

Bekker, M.G., 1969. Introduction to terrain-vehicle systems. University of Michigan Press, Ann Arbor. OCLC: 1919.

Bouton, A., Gao, Y., 2022. Crawling locomotion enabled by a novel actuated rover chassis. In: 2022 International Conference on Robotics and Automation (ICRA). IEEE Press, pp. 8164–8170. https://doi.org/10.1109/ICRA46639.2022.9811836.

Bouton, A., Reid, W., Brown, T., Daca, A., Sabzehi, M., Nayar, H., 2023. Experimental study of alternative rover configurations and mobility modes for planetary exploration. In: 2023 IEEE Aerospace Conference. IEEE, Big Sky, MT.

Cao, C., Creager, C., Lieu, D.K., Stuart, H.S., 2021. Mobility experiments assessing performance of front-back differential drive velocity on sandy terrain. In: ISTVS 2021, International Society for Terrain-Vehicle Systems, Virtual Conference.

Chhaniyara, S., Brunskill, C., Yeomans, B., Matthews, M., Saaj, C., Ransom, S., Richter, L., 2012. Terrain trafficability analysis and soil mechanical property identification for planetary rovers: A survey. J. Terrramech. 49, 115–128. https://doi.org/10.1016/j.jterra.2012.01.001. URL: https://linkinghub.elsevier.com/retrieve/pii/S002248981200002X.

Creager, C., Johnson, K., Plant, M., Moreland, S., Skonieczny, K., 2015. Push–pull locomotion for vehicle extrication. J. Terrramech. 57, 71–80. https://doi.org/10.1016/j.jterra.2014.12.001. URL: https://linkinghub.elsevier.com/retrieve/pii/S0022489814000937.

Daca, A., Skonieczny, K., 2022. Evaluating 1-g testing methods for predicting planetary rover mobility in reduced gravity. In: 16th Symposium on Advanced Space Technologies in Robotics and Automation (ASTRA) 2022, Noordwijk, the Netherlands.

Edwards, M.B., Dewoolkar, M.M., Huston, D.R., 2016. Geotechnical properties of fillite—simulant for planetary rover mobility studies. J. Aerospace Eng. 29, 04016022. URL: https://ascelibrary.org/doi/10.1061/(ASCE)AS.1943-5525.0000613, https://doi.org/10.1061/(ASCE)AS.1943-5525.0000613.

Gonzalez, R., Iagnemma, K., 2017. Slippage estimation and compensation for planetary exploration rovers. State of the art and future challenges. J. Field Robot. 35, 564–577. https://doi.org/10.1002/rob.21761. URL: https://onlinelibrary.wiley.com/doi/10.1002/rob.21761.

Huh, T.M., Cao, C., Aderibigbe, J., Moon, D., Stuart, H.S., 2023. Walk-Burrow-Tug: Legged anchoring analysis using RFT-based granular limit surfaces. IEEE Robot. Automat. Lett. 1–8. https://doi.org/10.1109/LRA.2023.3269324.

Li, C., Zhang, T., Goldman, D.I., 2013. A terradynamics of legged locomotion on granular media. Science 339, 1408–1412. https://doi.org/10.1126/science.1229163. URL: https://www.sciencemag.org/lookup/doi/10.1126/science.1229163.

Metzger, P.T., Anderson, S., Colaprete, A., 2018. Experiments indicate regolith is looser in the lunar polar regions than at the lunar landing sites. In: Earth and Space 2018. American Society of Civil Engineers, Cleveland, Ohio, pp. 79–85. https://doi.org/10.1061/9780784481899.009.

NASA, VIPER Mission Overview. URL: http://www.nasa.gov/viper/overview.

Moreland, S.J., 2013. Traction Processes of Wheels in Loose, Granular Soil. Ph.D. thesis. Carnegie Mellon University, Pittsburgh, PA.

Niksirat, P., Daca, A., Skonieczny, K., 2020. The effects of reduced-gravity on planetary rover mobility. Int. J. Robot. Res. 39, 797–811. https://doi.org/10.1177/0278364920913945. URL: http://journals.sagepub.com/doi/10.1177/0278364920913945.

Oravec, H.A., Asnani, V.M., Creager, C.M., Moreland, S.J., 2021. Geotechnical review of existing mars soil simulants for surface mobility. In: Earth and Space 2021, American Society of Civil Engineers, Virtual Conference. pp. 157–170. URL: https://ascelibrary.org/doi/10.1061/9780784483374.016, doi:10.1061/9780784483374.016.

Pérez del Pulgar Mancebo, C.J.P.d.P., Manrique, P.R., Delgado, G.J.P., Ibáñez, J.R.S., Azkarate, M., 2019. Choosing the Best Locomotion Mode in Reconfigurable Rovers. Electronics 8, 818. URL: https://www.mdpi.com/2079-9292/8/7/818, https://doi.org/10.3390/electronics8070818.

Schepelmann, A., Gerdts, S., 2022. Characterization of Infrared Optical Motion Tracking System in NASA's Simulated Lunar Operations (SLOPE) Laboratory. Technical Memorandum E-20035, NASA/TM-20220005304. NASA Glenn Research Center. URL: https://ntrs.nasa.gov/citations/20220005304.

Shirley, M., Balaban, E., Colaprete, A., Elphic, R.C., Sanchez, H., Falcone, L., Beyer, R., Banerjee, S., Bradner, K., 2022. VIPER Traverse Planning. In: 53rd Lunar and Planetary Science Conference, Lunar and Planetary Institute, The Woodlands, TX.

Shrivastava, S., Karsai, A., Aydin, Y.O., Pettinger, R., Bluethmann, W., Ambrose, R.O., Goldman, D.I., 2020. Material remodeling and unconventional gaits facilitate locomotion of a robophysical rover over granular terrain. Science Robot. 5, eaba3499. https://doi.org/10.1126/scirobotics.aba3499. URL: https://robotics.sciencemag.org/lookup/doi/10.1126/scirobotics.aba3499.

Skonieczny, K., Moreland, S.J., Asnani, V.M., Creager, C.M., Inotsume, H., Wettergreen, D.S., 2014. Visualizing and analyzing machine-soil interactions using computer vision: visualizing and analyzing machine-soil interactions using computer vision. J. Field Robot. 31, 820–836. https://doi.org/10.1002/rob.21510. URL: https://onlinelibrary.wiley.com/doi/10.1002/rob.21510.

Slonaker, J., Motley, D.C., Zhang, Q., Townsend, S., Senatore, C., Iagnemma, K., Kamrin, K., 2017. General scaling relations for locomotion in granular media. Phys. Rev. E 95, 052901. https://doi.org/10.1103/PhysRevE.95.052901. URL: http://link.aps.org/doi/10.1103/PhysRevE.95.052901.

Smith, K.E., Colaprete, A., Lim, D., Andrews, D., 2022. The VIPER mission, a resource-mapping mission on another celestial body. In: SRR XXII MEETING Colorado School of Mines.

Tolsa Industrial, Fillite Standard Grades - Industrial: Microesferas. URL: http://tolsaindustrial.com/microesferas/en/producto/fillite-the-all-round-solution-standard-grades/.

Treers, L.K., Cao, C., Stuart, H.S., 2021. Granular resistive force theory implementation for three-dimensional trajectories. IEEE Robot. Automat. Lett. 6, 1887–1894. https://doi.org/10.1109/LRA.2021.3057052. URL: https://ieeexplore.ieee.org/document/9345981/.

Agarwal, S., Karsai, A., Goldman, D.I., Kamrin, K., 2021. Surprising simplicity in the modeling of dynamic granular intrusion. Sci. Adv. 7, eabe0631. ISSN: 2375-2548. URL: https://www.science.org/doi/10.1126/sciadv.abe0631doi:10.1126/sciadv.abe0631.